

Article

A Radiological Approach to Evaluate Bone Graft Integration in Reconstructive Surgeries

Carlo F. Grottoli ¹, Riccardo Ferracini ^{2,*}, Mara Compagno ³, Alessandro Tombolesi ⁴, Osvaldo Rampado ⁴, Lucrezia Pilone ^{1,5}, Alessandro Bistolfi ⁶, Alda Borrè ⁴, Alberto Cingolani ¹ and Giuseppe Perale ^{1,2,7,*}

¹ Industrie Biomediche Insubri SA, Via Cantonale 67, 6805 Mezzovico-Vira, Switzerland; carlo.grottoli@ibi-sa.com (C.F.G.); lucrezia.pilone@gmail.com (L.P.); alberto.cingolani@ibi-sa.com (A.C.)

² Department of Surgical Sciences, Orthopaedic Clinic-IRCCS A.O.U. San Martino, 16132 Genova, Italy

³ Center for Research and Medical Studies, A.O.U. Città della Salute e della Scienza, 10129 Torino, Italy; mcompagno@cittadellasalute.to.it

⁴ Radiologia Diagnostica Presidio CTO, Azienda Ospedaliero-Universitaria Città della Salute e della Scienza di Torino, 10129 Torino, Italy; atombolesi@cittadellasalute.to.it (A.T.); orampado@cittadellasalute.to.it (O.R.); aborre@cittadellasalute.to.it (A.B.)

⁵ Department of Mechanical and Aerospace Engineering, Politecnico di Torino, Corso Duca degli Abruzzi 24, 10129 Torino, Italy

⁶ Department of Traumatology and Rehabilitation, C.T.O. Hospital-A.O.U. Città della Salute e della Scienza, 10129 Torino, Italy; abistolfi@cittadellasalute.to.it

⁷ Biomaterials Laboratory, Institute for Mechanical Engineering and Materials Technology, University of Applied Sciences and Arts of Southern Switzerland, Via Cantonale 2C, 6928 Manno, Switzerland

* Correspondence: riccardoferraciniweb@gmail.com (R.F.); giuseppe@ibi-sa.com (G.P.); Tel.: +41-(0)91-930-6640 (G.P.)

Received: 23 January 2019; Accepted: 1 April 2019; Published: 8 April 2019



Featured Application: This protocol allows tracking new bone formation after implantation of a xenohybrid bone graft (SmartBone®), without invasive histological samples.

Abstract: (1) Background: Bone tissue engineering is a promising tool to develop new smart solutions for regeneration of complex bone districts, from orthopedic to oral and maxillo-facial fields. In this respect, a crucial characteristic for biomaterials is the ability to fully integrate within the patient body. In this work, we developed a novel radiological approach, in substitution to invasive histology, for evaluating the level of osteointegration and osteogenesis, in both qualitative and quantitative manners. (2) SmartBone®, a composite xeno-hybrid bone graft, was selected as the base material because of its remarkable effectiveness in clinical practice. Using pre- and post-surgery computed tomography (CT), we built 3D models that faithfully represented the patient's anatomy, with special attention to the bone defects. (3) Results: This way, it was possible to assess whether the new bone formation respected the natural geometry of the healthy bone. In all cases of the study (four dental, one maxillo-facial, and one orthopedic) we evaluated the presence of new bone formation and volumetric increase. (4) Conclusion: The newly established radiological protocol allowed the tracking of SmartBone® effective integration and bone regeneration. Moreover, the patient's anatomy was completely restored in the defect area and functionality completely rehabilitated without foreign body reaction or inflammation.

Keywords: bone tissue regeneration; computed tomography; Xenografts

1. Introduction

In the last 50 years, remarkable advances have been made in the biomaterials field in general, including those for bone regeneration purposes [1]. In this respect, natural and synthetic materials [2] have evolved and are now able to properly replicate complex tissue structures, playing an active role in the repair and regeneration of bone defects [3,4].

Different approaches have been developed to mimic native tissue function [5,6]. One of the most successful one, is the use of porous scaffolds [7] that allow, initially, cell migration and nutrients diffusion, and afterwards provide structural support [8]. This way, cells can grow in the correct shape and location [9,10]. In this respect, certainly the usage of trabecular bone itself (i.e., bone grafts [11–14]) as a template, represent a major strategy, as its porous structure is already naturally suited for cell colonization [15,16]. Moreover, ideal scaffolds, together with biocompatibility, osteocompatibility, osteoconduction, osteoinduction, and neovasculogenic profile [17] should be resorbed or replaced once new bone has formed and they are no longer needed [14]. Apart from bone grafts, other resorbable scaffold constructs are generally composed of a collagen matrix [18], hyaluronan [19], and polymer-based [20,21] materials. If properly formulated [22], they also ensure, together with resorption profile that can be tailored to desired timeframe [23,24], adequate mechanical support [11,16,25] and promoted interactions between growth factors and progenitor cells allowing their proliferation and differentiation into various types [26,27].

In our study, we used SmartBone[®] (SB), a xeno-hybrid heterologous bone scaffold proved to have osteoconductive abilities [28–30] available on the market since 2012 as a CE-marked class III medical device (according to Directive 93/42/EEC of the European Union). Initially used only in the oral field [31–33], its integration with natural bone resulted to be efficient enough (averagely about one millimeter per month in the complex microenvironment of the mouth, characterized by high concentration of bacteria, which theoretically could limit its osteointegration and cell differentiation [34]) to be successfully extended to other areas [35,36]. As a matter of fact, nowadays, SB is used in the orthopedic field as well.

Together with post-marketing surveillance, in general, advanced clinical and biological analysis are of utmost importance in evaluating an implantable medical device's performance (European Commission guideline Med.Dev 2.7.1, Rev.4, June 2016). This way, in the case of resorbable grafts, it is possible to track whether natural restructuring has allowed the creation of biological tissue with optimized microstructure, according to the physiological function [37,38]. In this respect, certainly histological examinations represent a crucial analysis [39]. This technique involves tissue biopsy, which requires the collection of bone material from the patient [29,31,35]. As a consequence, it results to be an invasive practice and, although it can be carried out fairly smoothly in the oral field, it becomes rather difficult in the skull region or in the orthopedic one [40]. Another very important analysis is represented by *in vitro* studies that allow directly tracking the cell growth within the scaffold framework [30,41]. On the other hand, they have the limitation of being only partially representative of the actual performance upon implantation into the patient body.

Similar studies have already been performed on SB [29,30,41], providing a complete and detailed explanation of its integration mechanism over time on an averaged base, though not allowing the evaluation of each patient's specific situations. This was mostly due to the aforementioned difficulty in collecting tissue samples from the implantation site. In this respect, we focused, therefore, in developing a non-invasive method that allows an objective and quantitative analysis on the performance of the implanted SB without the surgical procedure for histological samples harvesting. That is, radiographically assessing the new bone formation and its volumetric increase directly in the graft site. Indeed, this can be nicely imaged through computed tomography (CT) [42,43], because native bone and SB have different densities. Therefore, they can be distinguished, and such differences measured by Hounsfield unit (HU).

We here developed a bioinformatical approach to build 3D models by CT scans and validated it evaluating bone regeneration in six individual patients, pre- and post- SB grafting, taking advantage

of CT. This represents a non-invasive method based on radiological examination only, used in compliance with the radioprotection principles of justification and optimization. This approach allowed patient-specific analysis of new bone formation over time, objectively and quantitatively: by overlapping CT models, we calculated the volumetric increase of new bone formation, recording higher volumes with respect to grafts after an average of 7 months post-surgery in all dental cases. Finally, apart from this quantitative analysis, we also investigated the density of the newly generated bone, as a read-out of bone quality: the obtained data shows that an average of 80% of bone remodeling occurs already after an average of 9 weeks post-surgery, hence, confirming the excellent performance of SB.

2. Materials and Methods

2.1. Scaffold Preparation

The bovine-derived xenohybrid composite bone scaffold SB was sourced as previously described, being certified for human use and of BSE/TSE (i.e., Bovine Spongiform Encephalopathy / Transmissible Spongiform Encephalopathy) free origin [44]. SB standard blocks, as well as custom-made SB blocks, were used in the surgical interventions, being the latter one also commercially traded under the name SmartBone® on Demand™ (SBoD) [35].

2.2. Clinical Investigations

Six patients were analyzed, and all of them underwent a surgical procedure with SB, receiving either standard blocks or custom-made blocks (Industrie Biomediche Insubri S/A, Mezzovico-Vira, Switzerland). Specifically, four patients underwent dental implants, one case underwent cranio-maxillo-facial (CMF) skull implants, and one case underwent orthopedic implant. Each case is described in detail hereby:

- Case #1: The first patient, 60-year-old female, showed hypodontia in the lower dental arch (three teeth in region 45, 46, 47 missing) and lack of a bone portion at diagnosis by Cone Beam CT (*a.k.a.* CBCT) (Figure 1a). Since a greater amount of bone was needed to carry out the dental implant, she underwent bone grafting with custom manufactured SBoD. The operating technique required a horizontal and vertical augmentation: bone defect did not have a simple shape, so a customized graft was required. By 3D reconstruction a model of the patient's mandibular bone was generated first, and then the missing bone component was designed (Figures S1 and S2 in Supplementary Materials). The missing pieces were also tested on a stereolithographic model. The surgical operation required an engraving into the gum to reach the alveolar bone. Next, the custom-made pieces of SB were positioned in the area where an increase of the amount of bone was needed. When the right position for the bone graft was found, it was fixed with screws, to allow the tight anchoring of the graft to the patient receiving bone. Furthermore, in the procedure of soft tissue closure over the implant, good care was taken to release the tissue flaps proximally using an elevator to obtain a tension free flap.
- Case #2: The second patient, 57-year-old female, smoker, showed partial edentulia and lack of bone and teeth from 21 to 27 throughout the upper right dental arch, as diagnosed by CBCT. The patient's jaw was rebuilt based on CT and surgeon cut SB standard blocks on a sterile 3D model of the patient's anatomy (Figure 1b). A "periosteal elevation" was further performed, a procedure by which the periosteum together with the soft tissues is removed from the bone, to allow the positioning of the customized SB graft. The custom-made block grafts were implanted within the bone defect area. Screws in the bone stabilized the graft. After checking the stability of the system and having the screws firmly positioned, the incision was sutured; soft tissues covered the bone graft, and the two gum flaps were sutured.
- Case #3: The third patient, 59-year-old female, showed severe edentulia with only two teeth left on the upper arch, at diagnosis by CBCT (Figure 1c). This loss of teeth has led to bone reabsorption,

and, thus, the lack of bone portion was deep. She underwent surgery, after custom made SBOD blocks were obtained. A periosteum elevation procedure was performed, as previously described. Additionally, before placing the graft in the bone defect area, the surface of the bone was micro-drilled to induce bleeding intending to further enhance the regenerative processes (*a.k.a.* micro-channeling practice). Then, the bone graft was implanted and stabilized by screws. After checking the stability of the system and having the screws firmly positioned, the dentist deposited an autologous platelet concentrate (PRP) to promote tissue healing. Lastly, the bone graft was covered by soft tissues. and the two flaps of the gum were sutured.

- Case #4: The fourth patient, 57-year-old male, showed four different bone defects as diagnosis by CBCT (Figure 1d). The periosteum disconnection procedure was performed, as described in previous cases. Once the bone was reached, the surgeon customized by hand SB standard blocks, that were implanted and firmly stabilized by screws. As in previous cases, the wound was finally closed on all its levels till external gums.
- Case #5: The fifth patient, 65-year-old female, showed a meningioma tumor located at the back of the right eye, diagnosed by CT (Figure 1e). The tumor included temporal and sphenoid bone in the skull. The surgical operation involved the removal of the tumor as well as part of two bones, which were rebuilt with custom-made SBOD grafts (Figure S3 in Supplementary Material). CT was used to design surgery, both in terms of tumor resection and further bone reconstruction. Given the wide extension of the tumor mass, a significant portion of bone had to be removed, and custom-made SB was provided in pieces, which were assembled during surgery, bed-side, and soaked into blood before grafting, to accelerate the osteointegration process [35]. Once placed, the complete graft has been stabilized with two small titanium plates (KLS-Martin, Germany).
- Case #6: The sixth case, 65-year-old male, presented a clear lack of bone in the distal left radial epiphysis of the left hand, at diagnosis by CT. For a better design of bed-side hand customized SB standard blocks, a 3D model where the bone defect was visible at the apex of the radial bone was built (Figure 1f). The surgical operation required the insertion of the SB block inside the defect during stabilization.

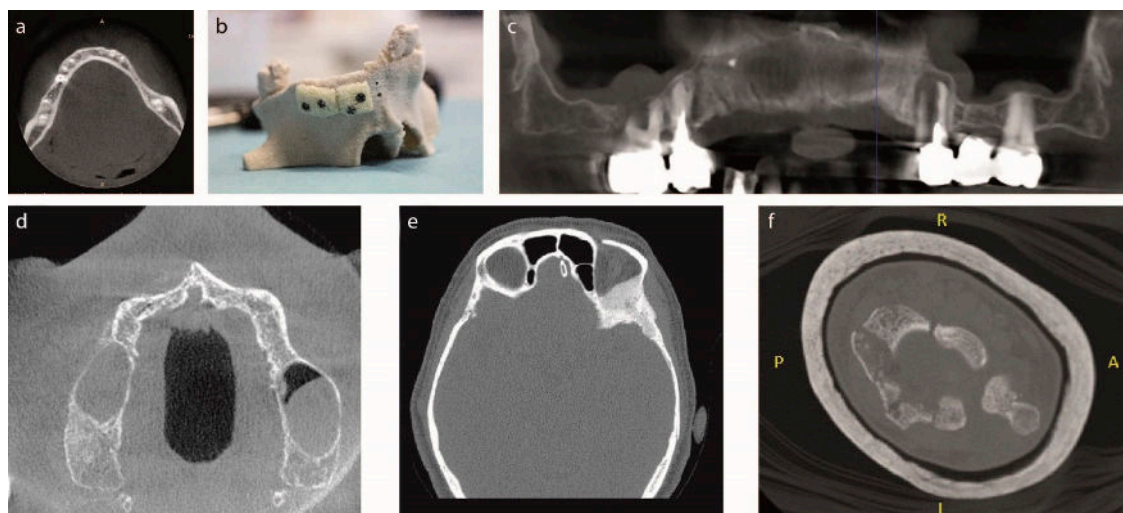


Figure 1. Initial conditions of the six investigated clinical cases. (a) Clinical case #1, patient with hypodontia in the lower dental arch; (b) Clinical case #2, sterile 3D real model of upper dental arch of partially edentulous patient, with bed-side hand cut SmartBone® blocks; (c) Clinical case #3, CBCT scan of upper arch of patient's severe edentulia; (d) Clinical case #4, CBCT scan of upper arch of patient's severe edentulia; (e) Clinical case #5, CT shows meningioma tumor located at the back of the right eye; (f) Clinical case #6, CT slice showing apex of the radial bone defect.

2.3. Computed Tomography (CT)

Table 1 shows radiological equipment and key settings used for image acquisition. For CBCT equipment, isotropic voxels are always intrinsically defined by the acquisition protocol, with dimensions ranging between 0.16 and 0.4 mm. For case #5 and #6, images were acquired with a multi slice computed tomography (MSCT), for which the pixel size is defined by the choice of the field of view combined with a standard 512×512 matrix, while the slice thickness is determined by the type of detector used. As part of a multi-planar and three-dimensional reconstruction from MSCT images, it is possible to reformat the voxels of the volume using reconstructions of partially overlapping tomographic sections. In any case, the spatial resolution will be lower than that commonly obtained with CBCT equipment.

The kilovolt and milliamperere radiological output parameters (associated with energy and intensity of the X-ray beam) are common values for the indicated equipment, defined to obtain an adequate level of contrast and image noise. For each case, the images used to evaluate the temporal variations of bone volume were acquired on the same scanner.

Table 1. Type of radiological equipment, manufacturer, and exposure parameters used for image acquisition of the six analyzed cases.

Cases	Radiological Equipment	Manufacturer	FOW Diameter (mm)	Pixel Size (mm)	Slice Thickness	Exposure Parameters
Case 1	CBCT	Imaging Science Int. I CAT	96	0.2	0.2	120 kV, 5 mA
Case 2	CBCT	Imaging Science Int. I CAT	85	0.4	0.4	120 kV, 5 mA
Case 3	CBCT	de Gotzen Acteon Group	104	0.2	0.2	85 kV, 8 mA
Case 4	CBCT	Sirona	82	0.16	0.16	85 kV, 7 mA
Case 5	CT	Toshiba	256	0.5	2	120 kV, 50 mA
Case 6	CT	GE	148	0.3	0.625	100 kV, 100 mA

2.4. 3D Virtual Reconstruction: Model Building

The 3D bone model reconstruction was carried out using the Mimics Innovation Suite by Materialise (Materialise HQ, Technologielaan 15, 3001 Leuven, Belgium).

Patients' CT scans are mandatory to perform a 3D reconstruction: indeed, results accuracy mostly relies on how the CT is carried out. Artefacts can compromise the quality of the 3D reconstruction. It is advisable to check that all CT slices are in order and sequential, and show a correct orientation (right-anterior-back) so that the 3D image can be designed correctly with respect to the reference system. The software Mimics converts the clinical images according to specific instructions regarding the orientation of the individual slices, and displays the CT from different levels (as shown in Figure S4 in Supplementary Material).

To obtain a usable 3D model, it is necessary to segment images according to the most common methods of image discretization. Digital filters are applied to enhance the quality of the images by performing high degree noise reduction, with the final goal of making the model the most identical possible to the anatomy of the patients.

Binomial blur filters are traditionally used to remove noise from images, by attenuating high spatial frequencies. A curvature flow filter performs an edge-preserving smoothing on the images. The discrete Gaussian filter computes the convolution of the image with a Gaussian kernel. It is used to smooth and reduce the image detail, preserving the edges for the low variance. Gradient magnitude is mainly used to help in the determination of object contours and separation of homogenous regions. The mena filter is commonly used for simple image noise reduction. The median filter is useful to reduce speckle noise and salt and pepper noise [45].

It is necessary to define a mask, which is created by a digitization process that allows to convert tissue analogic signals so that they can be processed with numerical calculation devices, by considering

the variation of the gray scale. A range of values is defined to represent a particular tissue: In our case, the adult compact bone range is around 500 to 2000 Hounsfield unit (HU) [46], while SmartBone[®] is in the range 100 to 400 HU. The gray value, defined in HU, precisely defines the tissue in each point. The HU is a value attributed to a voxel, which coincides to the average attenuation of the corresponding tissue volume. The choice of this range allows optimal tissue discrimination within the CT [47,48]. In some cases, this range value is modified to conceal the screws, to obtain a better view of SB and to have a better representation of the corresponding bone model.

Once the mask is created, it is possible to convert it into a 3D object. Next, the 3D model mesh quality is improved digitally by the software. If the model is highly consistent with the patient's anatomy no additional steps are required, otherwise, possible defects can be edited manually on the final model by the operator using 3-Matic, the CAD software of the Mimics Innovation Suite. It may be necessary to delete some artifacts that can be caused by poor CT quality or by the presence of metal implants or components that produce scattering. In those cases, a new definition of the slice contour on the slices of the CT scan is needed and Mimics software allow you to have many tools to correct those artefacts to obtain a consistent model.

2.5. Overlapping Models and Calculation of the Volumes

GOM Inspect (GOM GmbH, Braunschweig, Germany) is the software dedicated to the analysis of 3D measuring data for quality control, product development, and production. GOM software is used to evaluate 3D measuring data derived from GOM systems, 3D scanners, laser scanners, CTs and other sources, such as *STL (stereolithography file type, made basing on Standard Triangle Language)* models. The procedure of the overlapping of volumes is one among many possible methods to evaluate the volumetric bone growth that took place following the SB implant. Two 3D models are needed to perform the overlapping: The one built through pre-operation CT and the one constructed through post-operation CT.

Once models reproduce the patient's anatomy faithfully, it is possible to import the two geometric models into GOM Inspect to measure the differences between them. This image matching has to be done on images taken before the surgery *versus* those taken at least six months after when the patient is undergoing a control CT: Such timeframe allows seeing the beginning of the remodeling process supported by SB [29]. Moreover, this step overlap is necessary to get a comparison between the two models. The reference system of one model is converted into the reference system of the other model, to get a correct overlapping and avoid errors. It is very important to have a perfect alignment of the measuring model to the nominal model. Figure 2 shows an example of the pre-operative model imported as a mesh file (in gray) and the post-operative template imported as a CAD body file (in blue).

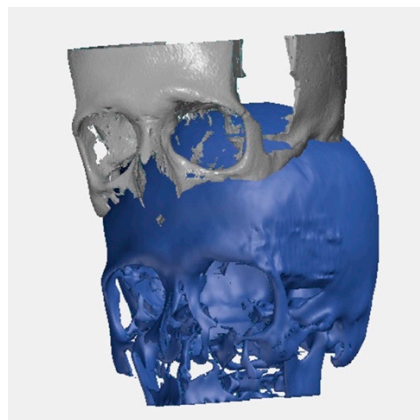


Figure 2. Example of the pre-operative model imported as a mesh file (in gray) and the post-operative template imported as a CAD body file (in blue).

It is crucial, in the overlapping procedure, to perform all possible alignment modes. Two types of alignment have been developed: 1) automatic pre-alignment and 2) alignments made by points. Pre-alignment is an automatic alignment created by the software through robust, effective algorithms. It works by recognizing three-dimensional features, such as edges or angles. Alignment by point consists of defining in the reference model a number of relevant anatomical points that are constant and also easily identifiable in the control model. The chosen points do not change in the two models enabling the chosen points to be perfectly aligned. After alignment, measurements are performed thanks to the GOM Inspects tools, which also provides the models' deviations and the measurements of increased bone volume (ΔV). That ΔV is the bone material regenerated from the SB graft.

The other method used to evaluate the volumetric bone growth is the Boolean subtraction between the two solid models. The software that carries out the subtraction is 3-Matic Medical (Materialise). With 3-Matic, the Boolean subtraction is performed on the 3D models obtained starting from two CT scans: one before the surgery and the other one always at least 6 months after the surgery. After an automatic alignment, the models obtained from the CT scan before surgery is subtracted from the model obtained from the CT scan after surgery. The software shows the remaining volume, which coincides with the bone regenerated (Figure 3).

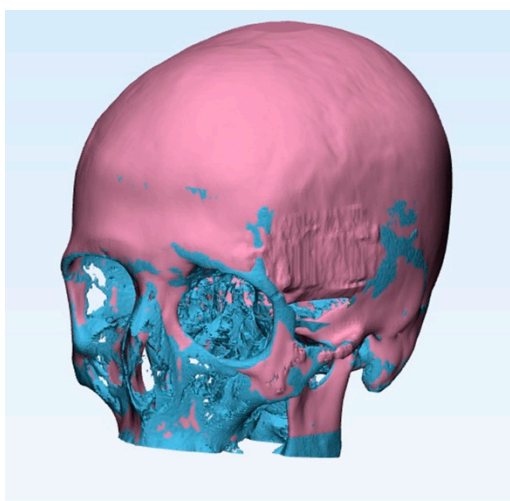


Figure 3. Example of the pre-operative model imported as a mesh file (in gray) and the post-operative template imported as a CAD body file (in blue).

3. Results

The cases included in the study were divided into two groups: The first group (1) included those cases in which the initial SB volume used during surgery was known, because they were custom-made implanted SB blocks (Table 2), hence, blocks designed and manufactured on demand specifically by the manufacturing company. The increase is considered with respect to the initial situation, i.e., the empty defect (considered as the 0 mm^3 reference); comparison is made between grafted SB (initial volume of SB) and final volumetric increase.

Table 2. Volumetric comparison on cases made with pre-customized SB blocks.

Cases	Region of Interest (ROI)	Final Volumetric Increase [mm^3]	Follow up Time	Initial Volume of SB [mm^3]
Case One	Dental	391	13 months	277
Case Three	Dental	605	6 months	781
Case Five	MCF	10,190	24 months	17831

The second group (2) included those other cases that did not have custom-made implants. Therefore, the surgeon had to cut and hand remodel standard blocks (Table 3). Here, again, the increase is considered with respect to the initial situation, i.e., the empty defect (considered as the 0 mm³ reference); comparison between grafted SB (initial volume of SB not known) and the final volumetric increase was, hence, not possible.

Table 3. Volumetric increase on cases made with handy customized SB blocks during surgery.

Cases	Region of Interest (ROI)	Volumetric Increase [mm ³]	Follow up Time
Case Two	Dental	605	8 months
Case Four	Dental	1028	14 months
Case Six	Orthopedic	1794	6 months

These last cases resulted in a lack of exact bone grafted volume information, and, thus, it was not possible to make a direct and precise comparison between the resulting volume and the initially implanted volume. Nevertheless, these cases are relevant given the intent of this work to assess these types of situations, being frequent in current common clinical practice.

Table 2 shows the volumetric increase in all studied cases with respect to initial conditions. Group 1 collects three cases in which the initial volume of SB is known. Moreover, in one dental case, the resulting volume was greater than the initial volume of implanted SB. Importantly, after 7 to 9 months the new bone always represented a large part of the volume (80.8%), and SB was almost completely reabsorbed (0.5%). These data were consistent with previous results from the literature [29].

Group 2 shows instead that all patients had new bone generation because in the pre-surgery CT a lack of bone was evident, and in post-surgery CT the defect is corrected by the formation of new bone. This could be established because native bone and SB have different densities. Therefore, they can be distinguished, and such difference can be measured by HU. This difference in density was particularly noticeable in case #5, hence, presented in Figure 4a,b, where the red circle (the defective bone) had a smaller white part (the newly formed bone) in the same area. This deduction was straightforward: New bone was clearly visible after two years post-surgery. Further details for each case are here described:

- **Case #1:** The patient responded well to the implant: By comparing the CT before the operation and the CT 13 months after surgery, a volumetric increase of 114 mm³ was calculated and no signs of inflammation. It was possible to proceed with the design of the dental implant, after checking that the body integrated the implant and the graft had allowed the regeneration of new bone. The project established dental implant positioning, which is important because they replaced the missing tooth roots. The surgery allowed the dentist to have the right plan specifications, for example, the distance between the teeth or the depth of the implant. One year later the patient still did not show any inflammation or foreign body reaction against implanted material so the implants could be fitted. They were implanted in the mandibular bone to create the base for the prosthesis crown that was fitted later on. The implants were ready to be attached to the abutment, which is the part connecting the implant to the crown. Moreover, it was evident that the graft maintained good stability for the implant, like natural bone. In Figure 5a, it is possible to observe the left mandible reconstruction. The anatomy of the new mandibular bone was highly similar to the healthy geometry (see the left part of the gray volume). This statement is supported by the fact that, if we divide the mandible with a sagittal plane in the center, we can compare the right part with the newly formed bone and check that both parts are symmetrically identical. On the other hand, in the gray part on the right, likely the bone was still regenerating because the natural geometry of the bone was not respected yet. In fact, symmetry, as regards the sagittal plane, has not occurred.
- **Case #2:** The patient responded very well to the implant: 8 months after the bone graft we calculated a volumetric increase of 142 mm³, with respect to the empty defect and no signs of

inflammation. In the upper dental arch, it was possible to observe the formation of new bone, which did not appear in the first CT (Figure 5b). At that time after 8 months, it was necessary to re-operate to remove the five screws implanted to proceed with the insertion of the dental implants. Next, the abutment was fitted to the implant by means of a screw to allow dental implant anchoring. If we divided the jaw with a sagittal plane, we could observe that the geometry was completely restored after eight months, because the left and the right part were symmetrical. In this case, the patient was ready for the dental implant because the bone thickness needed for the implant had been fully restored.

- Case #3: In this case, 6 months after the bone graft implantation, we could already observe the formation of new bone, not present in the first CT, as well as bone resurfacing even in parts where SB was not implanted (Figure 5c). In the upper dental arch, it was possible to detect the presence of the three screws, which ensured the stability of the bone graft. The two grafts could no longer be seen as they have been replaced by one reconstructed bone. Not only bone cells generated bone within SB but also osteogenesis occurred outside the grafts. There was a marked horizontal bone increase, which led to the correct anatomical shape being restored.
- Case #4: Follow ups of the patient were performed at different times, 6, 9, and 14 months, respectively. After 6 months post-surgery, the grafts appear to have filled the lack of bone (image not shown), with four screws stabilizing the bone grafts. The second follow up, 9 months after surgery, was performed to check whether the patient had complications. The tissue appears healthy and free of inflammation, and the graft was fully integrated into the patient's bone. At this point, the dentist could remove the screws that ensured stability. After 14 months, SB was completely replaced by the patient's bone. In Figure 5d, it is possible to observe how the bone was regenerated in all four points where SB was implanted. In the two central parts, where the lack of bone was more significant, the growth of the new bone was greater than in the other two parts. Notably, the grafts grew symmetrically and restored the natural anatomy of the maxillary bone.
- Case #5: After 11 days post-surgery a CT was performed to check the complete removal of the tumor and that the SB was integrating without causing foreign body reaction or inflammation. After 2 years post-surgery, osteointegration was fully successful, with the reconstruction of the temporal and sphenoid bone. The bone was perfectly regenerated, and the patient's cranial anatomy was completely reconstructed (Figure 5e). When we compared the two regions of interest in the post-surgery CT, we observed that the second one included a greater amount of bone. The bone was grown not only within the SB plaque but it was also remodeled to restore the correct skull anatomy; as a result, the right and left sides were symmetrical.
- Case #6: The patient underwent a CT after 5 months post-surgery to check whether the insertion of the SB was functional (image not shown). In the post-surgery CT, the little SB block grafted was visible, which was allowing the generation of new bone. Figure 5f shows the radius and the ulna: the bone not only grew within the SB but also around the graft, thus, completely filling the hole inside the epiphysis: The complete integration of the SB could be observed two years after surgery.

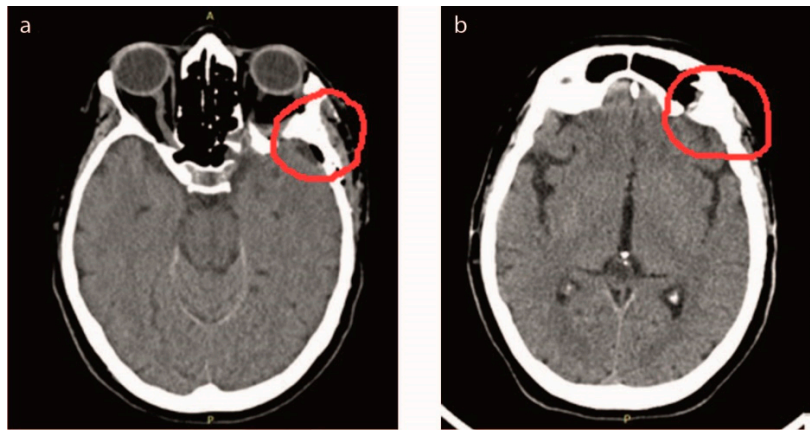


Figure 4. Clinical case #5; (a) CT slice immediately post-surgery, showing relatively low bone density, as highlighted in the graft area (red circle); (b) CT slice 2 years post-surgery, showing much higher signal, hence, higher bone density, due to new bone formation in the grafted region (red circle).

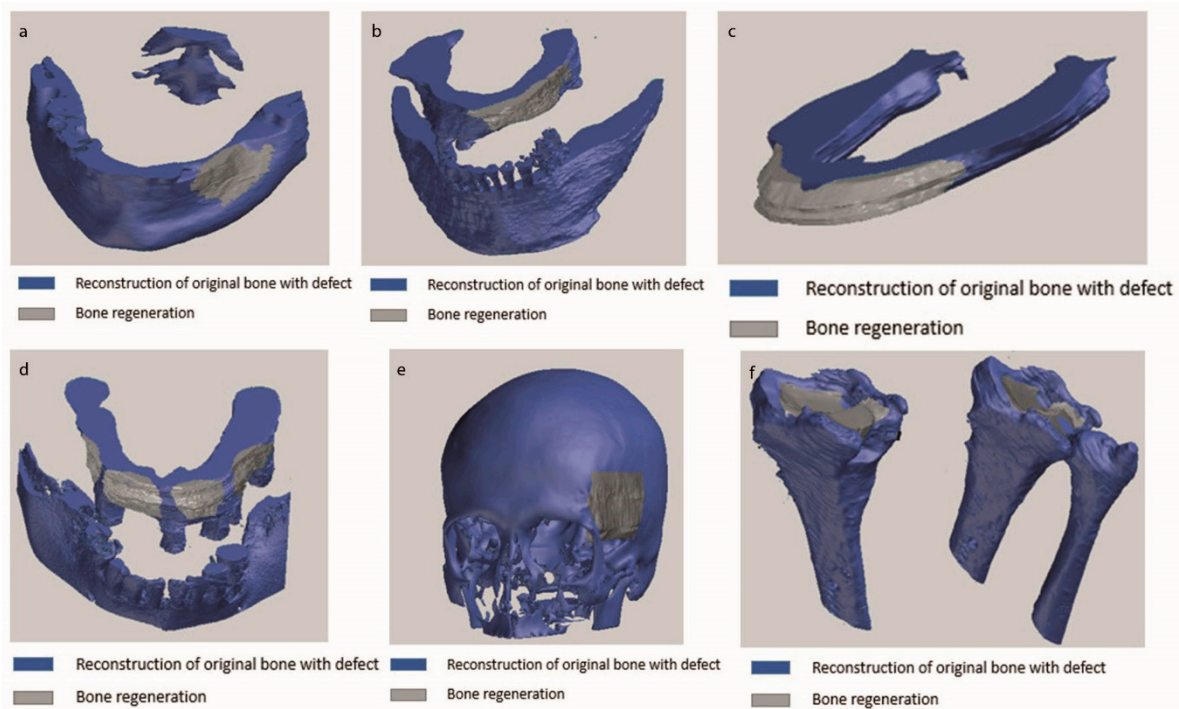


Figure 5. Follow-up images of the six investigated clinical cases; the gray area evidences the grafted volumes, indicated as bone regenerated volumes. (a) Clinical case #1, 13 months post-surgery reconstruction, volume stability is high and symmetry almost perfect. (b) Clinical case #2, 8 months post-surgery reconstruction, high volume stability of grafted SB. (c) Clinical case #3, 6 months post-surgery reconstruction, high volume stability and remodeling already in progress. (d) Clinical case #4, 14 months post-surgery reconstruction, excellent results on all SB grafted sites. (e) Clinical case #5, 24 months post-surgery reconstruction, complete graft integration and good symmetry. (f) Clinical case #6, 24 months post-surgery reconstruction, complete bone remodeling and restoration of functional anatomy.

4. Discussion

In the vast majority of cases, the quality of the new bone formation upon surgery is investigated through histology or densitometry, thus, implying a bone sampling from patient collected through a second operation. In our work, we have here proposed an innovative non-invasive method to establish a healthy bone volumetric increase after different time spans from the implant, which could be easily

used in follow up analyses. Specifically, to achieve this goal, the unique radiographic properties of SB have been exploited and were investigated to create 3D templates that faithfully mirrored the anatomy of the individual patient. The trickiest aspect of the applied method was to find the right way to make pre- and post- 3D models overlay accurately, because if the superimposition is precise, the volumetric increase should have respected the real anatomy. The overlay depends on the correct alignment of the 3D templates, and the pre-model reference system should change into the post-model reference one. We tested two different methods to evaluate the volumetric bone growth that took place following the SB implant. Both model-measuring methods used, by means of GOM and by Boolean subtraction with 3-matic, showed equivalent results and depended on the accurate creation of the models from the CT images. Hence, we decided to merge them. Indeed, the peculiarity of the final method is to create templates faithfully respecting the patient's anatomy by the two above mentioned alignments to obtain the best accurate overlapping, which could help us in the understanding the correct volumetric increase for all cases analyzed in the study.

As reasonably expected, the quality of the CT played a primary role in this radiological approach: A good quality yield provided a better resolution and a greater discretization of tissues as it allowed to calculate 3D models identical to the bone anatomical region and, consequently, to reach a more accurate calculation of the possible volumetric increase. Importantly, it has to be taken into account that the SB has low density allowing an optimal CT quality to be recognized.

The main technical aspects related to the acquisition and processing of CT images to obtain quantitative information on the skeletal system have recently been reviewed in Troy et al. [49], providing recommendations finalized to maximize the repeatability and objectivity of measurements. It is particularly important to perform the scans on the same equipment, standardizing the X-ray tube settings, the field of view and the slice thickness. To properly evaluate bone mineral density and distinguish components of integral, cortical, and trabecular bone, a calibration phantom with known hydroxyapatite density standards should be scanned together with the anatomical district of interest. This kind of phantom can reduce the effects of many error sources, such as change in acquisition settings, resolution, or those due to the scanner itself. It is also important to consider that voxel density values are less stable for CBCT equipment than MSCT, with noticeable variations even within the same scan for materials with homogeneous composition [50]. For these reasons, the quantitative method used in this study was limited to the assessments of compact bone volume, after appropriate segmentation, without further investigations about bone densities and composition. The determination of the threshold used for the extraction of bone volumes was not particularly critical given the high degree of separation with respect to the soft tissue densities, for all the considered equipment [49,50].

The developed novel radiological approach not only was successfully tested in a set of different cases related to different anatomical districts confirming its robustness but also allowed drawing conclusions on SB performances. In each analyzed case, good results were recorded: The geometry of the volumetric increase was similar or identical to the lack of bone in the injured area, and, importantly, the amount was expected, considering both post-surgery timing and defect shape. Independent experienced users judged the overlapping of the images to define the acceptable score: This explains minor displacements differences, by a few millimeters, between first and second alignment.

As expected, the volumetric increase was not the same in all patients because of both different investigated anatomical sites and different post-surgery times. Additionally, bone resorption also differed among patient as it depends on age and on other possible pathologies as well as on the size of the region where SB was grafted. Thus, although it was not possible to estimate the growth of SB at a given time, the results showed that this scaffold allowed the formation of new bone in all the examined cases, coherent with literature evidences. We also demonstrated a volumetric increase in each patient. Moreover, there is a clear morphological pattern on the evolution of the standard X-Ray imaging series over time which shows the substitution of the grafted material with a more homogeneous signal in the area of graft implant. The progressive remodeling together with an increase of the mineral signal cannot be dependent on the active remodeling of the graft *per se* given it is a decellularized matrix.

Therefore, the increase in the density over time must be dependent on novel mineral matrix apposition likely induced by the graft as previously shown in vitro [30]. This neo-apposition is quantified in the measures reported using CT scan. Indeed, clinically, partial increase of bone regeneration was already evident from CT scans performed 6 to 7 months post-surgery, likely due to the regeneration process ongoing, while obtained bone gain allows obtaining complete anatomy in a two-years timeframe averagely. Furthermore, bone growth was not only limited to the site where SB was inserted, but new bone was also growing in the areas adjoining the implant, suggesting that bone growth continued until the natural anatomy of the site was fully restored, further confirming SB mechanism of action.

Supplementary Materials: The following are available online at <http://www.mdpi.com/2076-3417/9/7/1469/s1>, Figure S1: Clinical case #1, patient with hypodontia in the lower dental arch, highlighted in red, Figure S2: Clinical case #1, patient with hypodontia in the lower dental arch; 3D render model of mandibular bone with the design of the custom made SmartBone® on Demand™ graft, Figure S3: Case #5, custom-made SBoD grafts built bed-side, prior to implantation, to reconstruct the temporal and sphenoid bones of the skull which had been previously removed due to the tumor, Figure S4: Exemplificative clinical images converted and displayed by Mimics software, according to specific instructions regarding the orientation of the individual slices.

Author Contributions: Conceptualization, C.F.G. and G.P.; methodology, C.F.G., A.T., O.R., A.B. (Alda Borrè); software, C.F.G., L.P., A.T., O.R.; validation, C.F.G., A.T., O.R., A.B. (Alda Borrè); formal analysis, G.P., R.F., A.B. (Alda Borrè); investigation, R.F., A.B. (Alda Borrè), A.B. (Alessandro Bistolfi); resources, G.P.; data curation, R.F., A.C., M.C.; writing—original draft preparation, all; writing—review and editing, G.P., A.C., M.C.; supervision G.P. and R.F.

Funding: This research received no external funding.

Conflicts of Interest: Giuseppe Perale is among shareholders of I.B.I. sa, the Swiss Company owning intellectual property rights on SmartBone®, manufacturing and commercializing it, including its custom-made line SmartBone® on Demand™, that was here investigated. Ing. Carlo Grottoli and Alberto Cingolani work for the same company. Riccardo Ferracini is an external clinical advisor to the same company. Ing. Lucrezia Pilone was involved as a guest master student, from Politecnico di Torino (Italy), by the same company at the time of this study.

Ethical Use of Clinical Data: All procedures were performed in strict accordance with the recommendations of the Declaration of Helsinki as revised in Fortaleza (2013) for investigations with human subjects, and followed good clinical practice and ISO14155 prescriptions. Study protocol was approved by the United Ethical Committee of the “Città della Scienza e della Salute”, Turin, Italy (approval n. 0004336). Informed consents have been recorded from all involved patients.

References

1. Planell, J.A. *Bone Repair Biomaterials*; Woodhead Publishing Limited: Shaston, UK, 2009; ISBN 9781845693763.
2. Sheikh, Z.; Sima, C.; Glogauer, M. Bone replacement materials and techniques used for achieving vertical alveolar bone augmentation. *Materials* **2015**, *8*, 2953–2993. [[CrossRef](#)]
3. Winkler, T.; Sass, F.A.; Duda, G.N.; Schmidt-Bleek, K. A review of biomaterials in bone defect healing, remaining shortcomings and future opportunities for bone tissue engineering. *Bone Joint Res.* **2018**, *7*, 232–243. [[CrossRef](#)] [[PubMed](#)]
4. Klouda, L.; Bouten, C.; Schenke-Layland, K. The Future of Tissue Engineering. *Curr. Opin. Biomed. Eng.* **2018**, *6*, iii–v. [[CrossRef](#)]
5. Stevens, B.; Yang, Y.; Mohandas, A.; Stucker, B.; Nguyen, K.T. A review of materials, fabrication methods, and strategies used to enhance bone regeneration in engineered bone tissues. *J. Biomed. Mater. Res. Part B Appl. Biomater.* **2008**, *85*, 573–582. [[CrossRef](#)] [[PubMed](#)]
6. Sarkar, S.K.; Lee, B.T. Hard tissue regeneration using bone substitutes: An update on innovations in materials. *Korean J. Intern. Med.* **2015**, *30*, 279–293. [[CrossRef](#)] [[PubMed](#)]
7. Ferracini, R.; Martínez Herreros, I.; Russo, A.; Casalini, T.; Rossi, F.; Perale, G. Scaffolds as Structural Tools for Bone-Targeted Drug Delivery. *Pharmaceutics* **2018**, *10*, 122. [[CrossRef](#)] [[PubMed](#)]
8. Roseti, L.; Parisi, V.; Petretta, M.; Cavallo, C.; Desando, G.; Bartolotti, I.; Grigolo, B. Scaffolds for Bone Tissue Engineering: State of the art and new perspectives. *Mater. Sci. Eng. C* **2017**, *78*, 1246–1262. [[CrossRef](#)]
9. Otsuki, B.; Takemoto, M.; Fujibayashi, S.; Neo, M.; Kokubo, T.; Nakamura, T. Pore throat size and connectivity determine bone and tissue ingrowth into porous implants: Three-dimensional micro-CT based structural analyses of porous bioactive titanium implants. *Biomaterials* **2006**, *27*, 5892–5900. [[CrossRef](#)]

10. Gupte, M.J.; Swanson, W.B.; Hu, J.; Jin, X.; Ma, H.; Zhang, Z.; Liu, Z.; Feng, K.; Feng, G.; Xiao, G.; et al. Pore size directs bone marrow stromal cell fate and tissue regeneration in nanofibrous macroporous scaffolds by mediating vascularization. *Acta Biomater.* **2018**, *82*, 1–11. [[CrossRef](#)]
11. Cingolani, A.; Grottoli, C.F.; Esposito, R.; Villa, T.; Rossi, F.; Perale, G. Improving Bovine Bone Mechanical Characteristics for the Development of Xenohybrid Bone Grafts. *Curr. Pharm. Biotechnol.* **2018**, *19*, 1005–1013. [[CrossRef](#)]
12. Bracey, D.; Seyler, T.; Jinnah, A.; Lively, M.; Willey, J.; Smith, T.; Van Dyke, M.; Whitlock, P. A Decellularized Porcine Xenograft-Derived Bone Scaffold for Clinical Use as a Bone Graft Substitute: A Critical Evaluation of Processing and Structure. *J. Funct. Biomater.* **2018**, *9*, 45. [[CrossRef](#)]
13. Guarnieri, R.; Belleggia, F.; DeVillier, P.; Testarelli, L. Histologic and Histomorphometric Analysis of Bone Regeneration with Bovine Grafting Material after 24 Months of Healing. A Case Report. *J. Funct. Biomater.* **2018**, *9*, 48. [[CrossRef](#)]
14. Bohner, M. Resorbable biomaterials as bone graft substitutes. *Mater. Today* **2010**, *13*, 24–30. [[CrossRef](#)]
15. Bignon, A.; Chouteau, J.; Chevalier, J.; Fantozzi, G.; Carret, J.P.; Chavassieux, P.; Boivin, G.; Melin, M.; Hartmann, D. Effect of micro- and macroporosity of bone substitutes on their mechanical properties and cellular response. *J. Mater. Sci. Mater. Med.* **2003**, *14*, 1089–1097. [[CrossRef](#)]
16. Hannink, G.; Arts, J.J.C. Bioresorbability, porosity and mechanical strength of bone substitutes: What is optimal for bone regeneration? *Injury* **2011**, *42*, S22–S25. [[CrossRef](#)]
17. Yuan, N.; Rezzadeh, K.S.; Lee, J.C. Biomimetic Scaffolds for Osteogenesis. *Recept Clin. Investig.* **2015**, 1–6. [[CrossRef](#)]
18. Salamanca, E.; Hsu, C.-C.; Huang, H.-M.; Teng, N.-C.; Lin, C.-T.; Pan, Y.-H.; Chang, W.-J. Bone regeneration using a porcine bone substitute collagen composite in vitro and in vivo. *Sci. Rep.* **2018**, *8*, 984. [[CrossRef](#)]
19. Chircov, C.; Grumezescu, A.M.; Bejenaru, L.E. Hyaluronic acid-based scaffolds for tissue engineering. *Rom. J. Morphol. Embryol.* **2018**, *59*, 71–76. [[CrossRef](#)]
20. Freed, L.E.; Vunjak-Novakovic, G.; Biron, R.J.; Eagles, D.B.; Lesnoy, D.C.; Barlow, S.K.; Langer, R. Biodegradable Polymer Scaffolds for Tissue Engineering. *Nat. Biotechnol.* **1994**, *12*, 1119–1124. [[CrossRef](#)]
21. Kroeze, R.J.; Helder, M.N.; Govaert, L.E.; Smit, T.H. Biodegradable polymers in bone tissue engineering. *Materials* **2009**, *2*, 833–856. [[CrossRef](#)]
22. Cingolani, A.; Casalini, T.; Caimi, S.; Klaue, A.; Sponchioni, M.; Rossi, F.; Perale, G. A Methodologic Approach for the Selection of Bio-Resorbable Polymers in the Development of Medical Devices: The Case of Poly(l-lactide-co- ϵ -caprolactone). *Polymers* **2018**, *10*, 851. [[CrossRef](#)]
23. Pertici, G.; Rossi, F.; Casalini, T.; Perale, G. Composite Polymer-Coated Mineral Grafts for Bone Regeneration: Material Characterisation and Model Study. *Ann. Oral Maxillofac. Surg.* **2014**, *2*, 1–7. [[CrossRef](#)]
24. Feng, P.; Wu, P.; Gao, C.; Yang, Y.; Guo, W.; Yang, W.; Shuai, C. A Multimaterial Scaffold With Tunable Properties: Toward Bone Tissue Repair. *Adv. Sci.* **2018**, *5*, 1–15. [[CrossRef](#)]
25. Sheikh, Z.; Najeeb, S.; Khurshid, Z.; Verma, V.; Rashid, H.; Glogauer, M. Biodegradable materials for bone repair and tissue engineering applications. *Materials* **2015**, *8*, 5744–5794. [[CrossRef](#)]
26. Fernandez de Grado, G.; Keller, L.; Idoux-Gillet, Y.; Wagner, Q.; Musset, A.-M.; Benkirane-Jessel, N.; Bornert, F.; Offner, D. Bone substitutes: A review of their characteristics, clinical use, and perspectives for large bone defects management. *J. Tissue Eng.* **2018**, *9*, 204173141877681. [[CrossRef](#)]
27. Haugen, H.J.; Lyngstadaas, S.P.; Rossi, F.; Perale, G. Bone grafts: Which is the ideal biomaterial? *J. Clin. Periodontol.* **2019**. [[CrossRef](#)]
28. Pertici, G.; Carinci, F.; Carusi, G.; Epistatus, D.; Villa, T.; Crivelli, F.; Rossi, F.; Perale, G. Composite Polymer-Coated Mineral Scaffolds for Bone Regeneration: From Material Characterization To Human Studies. *J. Biol. Regul. Homeost. Agents* **2015**, *29*, 136–148.
29. D'Alessandro, D.; Perale, G.; Milazzo, M.; Moscato, S.; Stefanini, C.; Pertici, G.; Danti, S. Bovine bone matrix/poly(L-lactic-co- ϵ -caprolactone)/gelatin hybrid scaffold (SmartBone[®]) for maxillary sinus augmentation: A histologic study on bone regeneration. *Int. J. Pharm.* **2017**, *523*, 534–544. [[CrossRef](#)]
30. Roato, I.; Belisario, D.C.; Compagno, M.; Verderio, L.; Sighinolfi, A.; Mussano, F.; Genova, T.; Veneziano, F.; Pertici, G.; Perale, G.; et al. Adipose-Derived Stromal Vascular Fraction/Xenohybrid Bone Scaffold: An Alternative Source for Bone Regeneration. *Stem Cells Int.* **2018**, *2018*, 1–11. [[CrossRef](#)]

31. Stacchi, C.; Lombardi, T.; Ottonelli, R.; Berton, F.; Perinetti, G.; Traini, T. New bone formation after transcrestal sinus floor elevation was influenced by sinus cavity dimensions: A prospective histologic and histomorphometric study. *Clin. Oral Implant. Res.* **2018**, 465–479. [[CrossRef](#)]
32. Spinato, S.; Galindo-Moreno, P.; Bernardello, F.; Zaffe, D. Minimum Abutment Height to Eliminate Bone Loss: Influence of Implant Neck Design and Platform Switching. *Int. J. Oral Maxillofac. Implant.* **2018**, 33, 405–411. [[CrossRef](#)]
33. Secondo, F.; Grottoli, C.F.; Zollino, I.; Perale, G.; Lauritano, D. Positioning of a Contextual Implant along with a Sinus Lift Anchored with a Block of Heterologous Bone. *Oral Implantol.* **2017**, 4, 457–467. [[CrossRef](#)]
34. Esposito, M.; Hirsch, J.-M.; Lekholm, U.; Thomsen, P. Biological factors contributing to failures of osseointegrated oral implants. *Eur. J. Oral Sci.* **1998**, 106, 527–551. [[CrossRef](#)]
35. Grecchi, F.; Perale, G.; Candotto, V.; Busato, A.; Pascali, M.; Carinci, F. Reconstruction of the zygomatic bone with smartbone®: Case report. *J. Biol. Regul. Homeost. Agents* **2015**, 29, 42–47.
36. Roato, I.; Belisario, D.C.; Compagno, M.; Lena, A.; Bistolfi, A.; Maccari, L.; Mussano, F.; Genova, T.; Godio, L.; Perale, G.; et al. Concentrated adipose tissue infusion for the treatment of knee osteoarthritis: Clinical and histological observations. *Int. Orthop.* **2018**. [[CrossRef](#)]
37. Taylor, D.; Hazenberg, J.G.; Lee, T.C. Living with cracks: Damage and repair in human bone. *Nat. Mater.* **2007**, 6, 263–268. [[CrossRef](#)]
38. Huiskes, R.; Rulmerman, R.; Van Lenthe, G.H.; Janssen, J.D. Effects of mechanical forces on maintenance and adaptation of form in trabecular bone. *Nature* **2000**, 405, 704–706. [[CrossRef](#)]
39. Jo, S.H.; Kim, Y.K.; Choi, Y.H. Histological evaluation of the healing process of various bone graft materials after engraftment into the human body. *Materials* **2018**, 11, 714. [[CrossRef](#)]
40. An, H.Y.; Martin, K.L. *Handbook of Histology Methods for Bone and Cartilage*; Springer Science+Business Media: New York, NY, USA, 2003.
41. Mayer, Y.; Ginesin, O.; Khutaba, A.; Machtei, E.E.; Zigdon Giladi, H. Biocompatibility and osteoconductivity of PLCL coated and noncoated xenografts: An in vitro and preclinical trial. *Clin. Implant. Dent. Relat. Res.* **2018**, 20, 294–299. [[CrossRef](#)]
42. Beaman, F.D.; Bancroft, L.W.; Peterson, J.J.; Kransdorf, M.J.; Menke, D.M.; James, K. Imaging Characteristics of Bone Graft Materials. *Radiographics* **2006**, 373–389. [[CrossRef](#)]
43. Bolland, B.J.R.F.; Kanczler, J.M.; Dunlop, D.G.; Oreffo, R.O.C. Development of in vivo μ CT evaluation of neovascularisation in tissue engineered bone constructs. *Bone* **2008**, 43, 195–202. [[CrossRef](#)]
44. Pertici, G. Bone Implant Matrix and Method of Preparing the Same. EP Patent EP2358407A1, 24 August 2011.
45. Senthilraja, S.; Suresh, P.; Suganthi, M. Noise Reduction in Computed Tomography Image Using WB – Filter. *Int. J. Sci. Eng. Res.* **2014**, 5, 243–247.
46. Fat, D.L.; Kennedy, J.; Galvin, R.; O'Brien, F.; Grath, F.M.; Mullett, H. The Hounsfield value for cortical bone geometry in the proximal humerus—an in vitro study. *Skelet. Radiol.* **2012**, 41, 557–568. [[CrossRef](#)]
47. Schreiber, J.J.; Anderson, P.A.; Hsu, W.K. Use of computed tomography for assessing bone mineral density. *Neurosurg. Focus* **2014**, 37, E4. [[CrossRef](#)]
48. Langton, C.M.; Njeh, C.F. *The Physical Measurement of Bone*; Institute of Physics Publishing Bristol and Philadelphia: Bristol, UK, 2003; ISBN 9781420033342.
49. Troy, K.L.; Edwards, W.B. Practical considerations for obtaining high quality quantitative computed tomography data of the skeletal system. *Bone* **2018**, 110, 58–65. [[CrossRef](#)]
50. Molteni, R. Prospects and challenges of rendering tissue density in Hounsfield units for cone beam computed tomography. *Oral Surg. Oral Med. Oral Pathol. Oral Radiol.* **2013**, 116, 105–119. [[CrossRef](#)]

